第 43 卷 第 13 期/2023 年 7 月/光学学报 研究论文

光学学报

非相干泵浦辅助的电磁诱导非厄密衍射光栅

田雪冬[1]，刘星雨[2]，刘一谋[2*]

[1]广西师范大学物理科学与技术学院，广西 桂林 541004；

[2]东北师范大学量子科学中心，吉林 长春 130024

摘要 提出一种基于非相干泵浦辅助的非厄密电磁诱导光栅的理论方案，其中物理系统由具有三能级Lambda型结构的超冷原子系综与非相干泵浦场组成。该方案仅通过单重空间周期调制便可获得光学宇称-时间对称和宇称-时间反对称等非厄密光学对称性。通过对探测光束透过该系统的远场衍射特性的研究发现：首先，通过非相干泵浦速率与控制光束失谐的操控可以实现不同非厄密光学对称性的切换；其次，在光学深度不变的前提下，可以通过非相干泵浦场对系统的衍射效率进行有效调制，从而引入全新的操控自由度；此外，控制光束失谐的相位可以有效操控系统的衍射对称性及衍射模式。该理论研究结果可以促进非厄密光学与散射型全光器件的研究与开发，并应用于量子光学与量子信息处理等领域。

关键词 衍射与光栅；电磁诱导透明；非厄密光学；非相干泵浦；衍射光栅；非对称衍射

中图分类号 O431.2；O436.1 **文献标志码** A **DOI**：10.3788/AOS230492

1 引 言

非厄密光学结构[1]是模拟非厄密物理系统[2]的重要物理平台和当前的研究热点之一。近年来，已经陆续在离散型光学系统，如光波导[3-5]、混合光学微腔[6-7]、电路谐振器[8]以及具有空间周期性调制的冷原子系综等连续型光学介质[9-13]中实现光学非厄密对称性。目前的非厄密光学系统的尺度在介观或宏观领域，使实验操控成为可能，而微观领域非厄密结构在光学平台实现需要在纳米以下的尺度对折射率进行调节，较为困难。非厄密光学系统展现出大量新颖的光学现象，如光学布洛赫振荡[14-15]、光子声子激光[16-17]、单向/双向光学不可见性和光学斗篷[18-23]等。

衍射光栅作为光谱分析和光学成像的重要工具，在物理学、化学、天文学、生物学等许多领域都发挥着重要作用。电磁诱导透明(EIT)[24]的电磁诱导光栅(EIG)[25]的出现，使衍射图案的动态控制成为可能。具有传统振幅/相位调制和非传统调制(非线性或非局域调制)的混合EIG方案改善了衍射效率并拓展了光栅的功能[26-29]。近年来，结合非厄密光学调制，许多非对称衍射方案已被初步提出[30-37]，甚至类似的非对称散射已在声学领域得到应用[38]。

然而，相较于使用离散型光学介质的非厄密光栅，基于负折射率连续变化的连续型非厄密光栅系统(如相干耦合的原子系统、光晶格等)的制备，均需要双重或多重周期调制(至少两个驻波场或一个驻波场结合周期性原子晶格)，同时提供非厄密对称性(宇称-时间对称或宇称-时间反对称)与衍射所需的空间周期性[30-37]。一方面，此类方案中的非厄密光学对称性的实现，要求多个参数共同配合，因此相较于离散型非厄密光学系统其制备复杂度高。另一方面，此类系统的非厄密光学对称性对参数较为敏感，易发生对称性破缺，不利于系统光学性质的动态调控，且缺少操控自由度，从而失去了相对于离散型非厄密光学系统的优势。因此急需一种制备复杂度不高兼具灵活操控特点的连续型非厄密光栅方案。

本文基于非相干泵浦辅助的单重周期空间调制的三能级超冷原子系统，提出了实现具有非厄密光学对称性的电磁诱导光栅的理论方案。并研究了该方案下，光栅的几种非对称衍射模式以及光学深度、非相干泵浦、控制场失谐及其初始相位等因素对光栅衍射性质的影响和调控。单重空间周期调制降低了非厄密光学系统制备的复杂度，而非相干泵浦的引入也为非对称衍射系统的全光控制提供了新的光栅调控自由度。

收稿日期：2023-02-03；**修回日期**：2023-02-26；**录用日期**：2023-03-06；**网络首发日期**：2023-03-13

基金项目：国家自然科学基金(12104107)、吉林省自然科学基金(20220101009JC)、中央高校基本科研业务费专项资金(2412022ZD046)、广西师范大学骨干教师海外研修“育才工程”

通信作者：*liuym605@nenu.edu.cn

2　基本原理

2.1　理论模型

考虑具有等效三能级Λ型结构的冷原子系统，其中每个原子均由基态$|g\rangle$、亚稳态$|m\rangle$以及激发态$|e\rangle$构成。如图1(a)所示，光学跃迁$|g\rangle\leftrightarrow|e\rangle$与$|m\rangle\leftrightarrow|e\rangle$分别由频率为$\omega_p$和$\omega_c$的相干光场耦合，相应光场的半拉比频率分别为$\Omega_p=\mu_{ge}\cdot E_p/2\hbar\varepsilon_0$和$\Omega_c=\mu_{em}\cdot E_c/2\hbar\varepsilon_0$（$\mu_{ge}$与$\mu_{em}$为相应的跃迁偶极矩）。此外在能级$|g\rangle$与$|e\rangle$之间额外施加速率为$\Lambda_{icp}$的非相干泵浦场。在电偶极近似与旋转波近似下，相互作用表象下的哈密顿量表示为$H_I=H_0+\mathcal{V}_{af}$，其中H_0为自由项，$\mathcal{V}_{af}$为场与原子相互作用项，具体形式为

$$H_0=\hbar\sum_j^N(\Delta_p\sigma_{ee}^j+\delta\sigma_{mm}^j)\ \mathcal{V}_{af}=\hbar\sum_j^N(\Omega_p\sigma_{eg}^j+\Omega_c\sigma_{em}^j)+h.c.\ ,\tag{1}$$

式中：$\sigma_{\mu\nu}^j$为第j个原子的投影（$\mu=\nu$）或跃迁算符（$\mu\neq\nu$）；$\Delta_p=\omega_{eg}-\omega_p$与$\delta=\Delta_p-\Delta_c$分别为单光子与双光子失谐（$\Delta_c=\omega_{em}-\omega_c$）。代入马尔可夫主方程$\frac{\partial\rho}{\partial t}=-\frac{i}{\hbar}[H_I,\rho]+\Lambda\rho$，$\Lambda$代表包括非相干泵浦、自发辐射与相干弛豫的耗散项，随即可以得到各密度矩阵元的动力学方程分别为

$$\dot{\rho}_{gg}=-\Lambda_{icp}\rho_{gg}+\Gamma_{eg}\rho_{ee}-i(\Omega_p\rho_{ge}-\Omega_p^*\rho_{eg}),\dot{\rho}_{mm}=\Gamma_{em}\rho_{ee}-i(\Omega_c\rho_{me}-\Omega_c^*\rho_{em}),\dot{\rho}_{eg}=-\left[\gamma_{ge}+i\Delta_p\right]\rho_{eg}-i\left[\Omega_p(\rho_{ee}-\rho_{gg})-\Omega_c\rho_{mg}\right],\dot{\rho}_{em}=-[\gamma_{me}+i\Delta_c]\rho_{eg}-i[\Omega_c(\rho_{ee}-\rho_{mm})-\Omega_p\rho_{gm}],\dot{\rho}_{gm}=-[\gamma_{gm}-i\delta]\rho_{gm}-i[\Omega_c\rho_{ge}-\Omega_p^*\rho_{em}]\tag{2}$$

式中：Γ_{eg}和Γ_{em}为自发弛豫速率；γ_{ge}、γ_{me}与γ_{gm}分别为该系统中的相干弛豫速率$\left[\gamma_{\mu\nu}=\left(\sum_k\Gamma_{\mu k}+\sum_k\Gamma_{\nu k}\right)/2,k\in\{g,e,m\}\right]$。方便起见，在下面的讨论中取$\Gamma_{eg}\simeq\Gamma_{em}=\gamma,\gamma_{me}=\gamma_0$。在弱探测极限下，求得$\rho_{eg}$的一阶稳态解为

$$\rho_{eg}(\Delta_p)=-\Omega_p\frac{(\Lambda_{icp}-2\gamma)\gamma_0\gamma A+|\Omega_c|^2[2(\Lambda_{icp}-\gamma)A-iB]}{\{2(2\Lambda_{icp}+\gamma+3\gamma_0)|\Omega_c|^2+\gamma[2\gamma\gamma_0+\Lambda_{icp}(\gamma+\gamma_0)]\}[A(\Delta_p-i\gamma)-|\Omega_c|^2]},\tag{3}$$

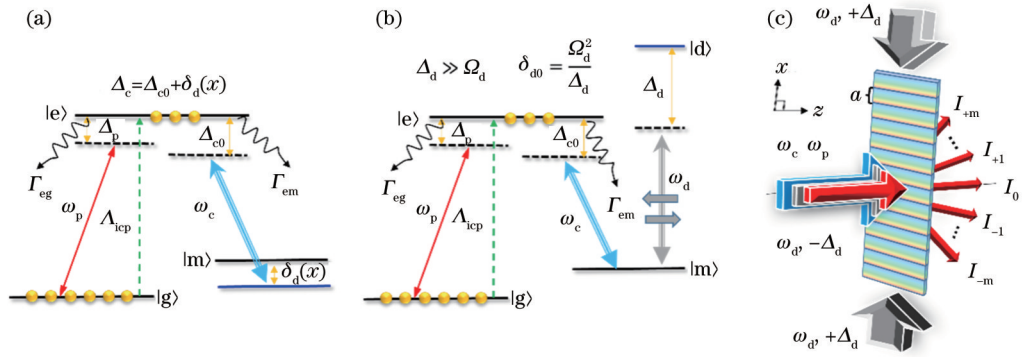

图1　等效三能级原子结构、实际能级结构以及准一维电磁诱导光栅的示意图。(a)等效三能级原子结构；(b)实际能级结构；(c)准一维电磁诱导光栅

Fig. 1　Schematic diagrams of atomic equivalent three level structure, actual energy structure, and quasi one-dimensional electromagnetically induced grating. (a) Atomic equivalent three level structure; (b) actual energy structure; (c) quasi one-dimensional electromagnetically induced grating

式中：$A=\Delta_p-i\gamma_0$；$B=\Lambda_{icp}(\gamma-\gamma_0)+2\gamma\gamma_0$。那么系统的线性极化率可以表示为$\chi(\Delta_p)=\alpha\rho_{eg}(\Delta_p)$，其中$\alpha=N\mu_{eg}^2/2\hbar\varepsilon_0\Omega_p$，$N$代表原子密度。

2.2　非厄密电磁诱导光栅与非对称衍射

接下来对控制场失谐引入空间周期性调制[10-11]，如图1(b)所示，采用文献[11]的方法，用一对远失谐的驻波场Ω_d耦合亚稳态$|m\rangle$与辅助激发态$|d\rangle$。远失谐条件$\Delta_d\gg\Omega_d$使得辅助态$|d\rangle$与系统解耦，但亚稳态$|m\rangle$获得了$\delta_{d0}=\frac{\Omega_d^2}{\Delta_d}$的斯塔克位移（AC Stark shift）。若利用一束沿z轴传播的行波场$E_d\exp[+ik_dz]$（失谐为$-\Delta_d$）与一对沿与x轴夹角分别为θ_d与$-\theta_d$传播的驻波场$(E_d/\sqrt{2})\exp[+i(k_d'x+\psi_d)]$，$(E_d/\sqrt{2})\exp[-i(k_d'x+\psi_d)]$（失谐为$+\Delta_d$）相干叠加，得到空间周期调制$\delta_d(x)=\frac{\Omega_d^2(x)}{\Delta_d}=\delta_{d0}\sin\left[2k_d'(x-x_0)+2\left(\psi_d-\frac{\pi}{4}\right)\right]$。这里$\Omega_d=E_d\mu_{dm}/2\hbar\varepsilon_0$为半拉比频率，$k_d'=k_d\cos\theta_d$与$k_d=\frac{2\pi}{\lambda_d}$分别为$x$方向波矢投影与波矢，$\psi_d$为驻波场的初始相位，$\psi_d-\frac{\pi}{4}$是波谷与系统光轴$x=x_0$的位置之差的等效初始相位。不妨令$\delta_c=\delta_d$且$\delta_{c0}=\delta_{d0}$，则在辅助态$|d\rangle$与

系统解耦时，此斯塔克位移可以合并计入等效控制场失谐中，即 $\Delta_c(x)=\Delta_{c0}+\delta_{c0}\sin\left[\frac{4\pi}{a}(x-x_0)+\phi\right]$，这里 $\phi=2\varphi_d-\frac{\pi}{2}$ 即有效耦合场 Ω_c 的失谐相位（以下简称耦合场失谐相位），$a=\frac{\lambda_c}{\sin\theta_d}$ 为驻波场 Ω_d 的空间周期（取 $\lambda_c\approx\lambda_d$）。在实际实验中，可以通过控制两束反向传播的辅助场 Ω_d 的初始相位 φ_d 来改变驻波场 Ω_d 的波节位置，进而调节耦合场失谐相位 ϕ 的大小。

由于频率扫描的双光子共振条件为 $\delta=\Delta_p+\Delta_c=0$，所以探测场感受到的介质极化率也带有空间周期性 $\chi(\Delta_p)=\chi(-\Delta_c)=\chi(x)$。探测场传出长度为 L 的原子介质后的透射率表示为

$$T(x)=\mathrm{e}^{\frac{-2\pi L}{\lambda_p}\chi''(x)}\cdot\mathrm{e}^{\frac{\mathrm{i}2\pi L}{\lambda_p}\chi'(x)},\tag{4}$$

式中，$\chi'(x)$ 与 $\chi''(x)$ 分别代表极化率的实部和虚部。已知稀薄原子气体复折射率 $n=n'+\mathrm{i}n''$ 与极化率之间的关系为 $n=\sqrt{1+\chi}\simeq1+\chi/2$，若极化率实部与虚部分别为空间坐标 x 的偶函数与奇函数，易得 $n'(-x)=-n'(x)$ 且 $n''(-x)=-n''(x)$，此时系统满足光学宇称-时间对称（PT symmetry）；类似地，若极化率实虚部分别为空间坐标 x 的奇函数和偶函数，易得 $n'(-x)=-n'(x)$ 且 $n''(-x)=n''(x)$，此时系统满足光学宇称-时间反对称（PT anti symmetry）。不论周期性的光学 PT 对称还是光学 PT 反对称均属于反相的空间周期调制（out-of-phase）。随后通过对 $T(x)$ 进行傅里叶变换，可以得到夫琅禾费（Fraunhofer）或者远场衍射方程为

$$\begin{cases}I_p=|\mathcal{E}(\theta)|^2\dfrac{\sin^2(M\pi\sin\theta)}{M^2\sin^2(\pi R\sin\theta)}\\ \mathcal{E}(\theta)=\displaystyle\int_{-a/2}^{+a/2}T(x)\mathrm{e}^{-\mathrm{i}2\pi xR\sin\theta}\mathrm{d}x\end{cases},\tag{5}$$

式中：$R=a/\lambda_p$；θ 是探测场经过衍射后与 z 方向成的夹角；M 是常数因子，代表空间探测光束宽度与光栅空间周期的比值。而第 m 级衍射级次则定义为 $m=R\sin\theta$，$m\in\{\cdots,-2,-1,0,+1,+2,\cdots\}$。

衍射强度的峰值出现在角度 θ_m 处，$k_m=k_p\sin(\theta_m)=2m\pi/a$。结合式（4），聚焦在第 m 级衍射级次上，此时 $E_m=E(\theta_m)$（$m\neq0$）。简便起见，令 $a(x)=\frac{2\pi L}{\lambda_p}\chi''(x)$，$b(x)=\frac{2\pi L}{\lambda_p}\chi'(x)$，于是可以对式（5）做泰勒级数展开：

$$E_m=\int_{-a/2}^{+a/2}\mathrm{d}x\cdot\mathrm{e}^{-\mathrm{i}2m\pi x}\left[1+a(x)+\frac{a(x)^2}{2}+\ldots+\frac{a(x)^{m_a}}{m_a!}\cdots\right]\left[1+\mathrm{i}b(x)-\frac{b(x)^2}{2}+\cdots+\frac{\left[\mathrm{i}b(x)\right]^{m_b}}{m_b!}\cdots\right],\tag{6}$$

当 $a(x)$ 与 $b(x)$ 远小于 1 时，定义

$$h'_m=\int_{-a/2}^{+a/2}\mathrm{d}x\cdot\left[1+a(x)+\frac{a(x)^2}{2}\right]b(x)\sin(2m\pi x)\quad h''_m=\int_{-a/2}^{+a/2}\mathrm{d}x\cdot\left[1+a(x)+\frac{a(x)^2}{2}\right]b(x)\cos(2m\pi x)\quad g'_m=\int_{-a/2}^{+a/2}\mathrm{d}x\cdot\left[1+a(x)+\frac{a(x)^2}{2}\right]\frac{b(x)^2-2}{2}\cos(2m\pi x)\quad g''_m=\int_{-a/2}^{+a/2}\mathrm{d}x\cdot\left[1+a(x)+\frac{a(x)^2}{2}\right]\frac{b(x)^2-2}{2}\sin(2m\pi x),\tag{7}$$

并作 $b(x)\to\varepsilon_m b(x)$ 的替换，当散射因子 ε_m 足够小时，可以仅保留到对应的二阶项[39]从而得到：

$$\begin{cases}E_m\simeq(h'_m\varepsilon_m-g'_m\varepsilon_m^2/2)+\mathrm{i}(h''_m\varepsilon_m-g''_m\varepsilon_m^2/2)\\ I_{\pm m}\simeq|h'_m\varepsilon_m\mp g'_m\varepsilon_m^2/2|^2+|h''_m\varepsilon_m\pm g''_m\varepsilon_m^2/2|^2\end{cases}。\tag{8}$$

不难发现，光学系统极化率的实部与虚部处于同相调制时（in-phase），即 $a(x)=a(-x)$ 且 $b(x)=b(-x)$，满足 $I_m=I_{-m}$ 对称衍射条件。相反地，当光学系统处于 PT 对称或者 PT 反对称这种反相调制（out-of-phase）时，一阶散射项的实部 h'_m、虚部 h''_m 以及二阶散射项的实部 g'_m、虚部 g''_m 均带有不尽相同的空间奇偶性。以 PT 反对称为例，由于 $a(x)=a(-x)$ 且 $b(x)=-b(-x)$，易知 $h'_m=-h'_{-m}$，$h''_m=h''_{-m}$，$g'_m=g'_{-m}$ 以及 $g''_m=-g''_{-m}$，进而得到第 $+m$ 级与 $-m$ 级衍射强度之差为 $I_m-I_{-m}\propto|h'_m g'_m-h''_m g''_m|\neq0$，即此时探测光经过该系统后发生了非对称衍射。

3 分析与讨论

下面分别讨论非相干泵浦辅助下非厄密电磁诱导光栅在几种不同衍射模式下的衍射特性。选取超冷 ^{87}Rb 原子的参数：$|g\rangle\equiv5S_{1/2}|F=1\rangle$，$|e\rangle\equiv P_{1/2}|F=2\rangle$，以及 $|m\rangle\equiv S_{1/2}|F=2\rangle$。退相干弛豫速率为 $\gamma_{ge}\simeq\gamma_{ge}=\gamma=2\pi\times5.9\,\mathrm{MHz}$，$\gamma_0\simeq3.0\,\mathrm{kHz}$。此外，假定原子长度取 $L=200\,\mu\mathrm{m}$，原子密度 $N=5.0\times10^{11}\,\mathrm{cm}^{-3}$，$R=2$ 以及 $M=10$。

3.1 宇称-时间对称光栅

计算得到结果如图 2（a）所示，当非相干泵浦速率为 $\Lambda_{icp}=2.0\times2\pi\,\mathrm{MHz}$，其他参数设置为 $\Delta_p=-2.27\times2\pi\,\mathrm{MHz}$、$\Delta_{c0}=-0.1\times2\pi\,\mathrm{MHz}$、$\delta_{c0}=1.0\times2\pi\,\mathrm{MHz}$ 以及 $\phi=0$ 时，可得到宇称-时间对称的极化率，表现为极化率实部（点线）与虚部（实线）分别为空间位置 x 的偶函数与奇函数，即 $\chi'(-x)=\chi'(x)$

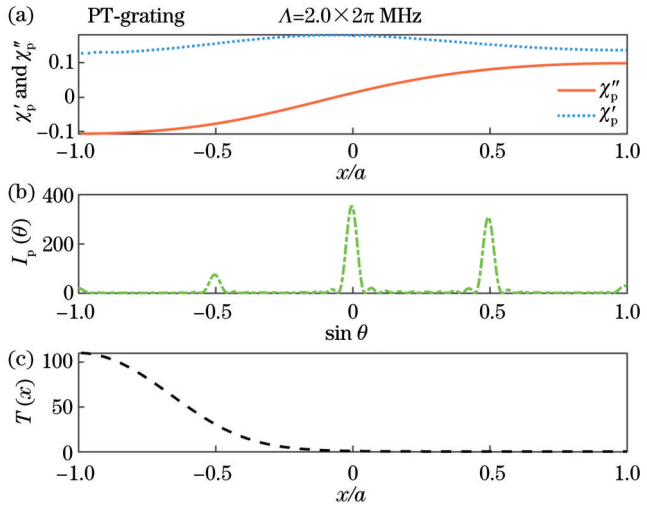

图 2　宇称-时间对称光栅衍射性质。(a)吸收(实线)与色散(点线)谱;(b) 光栅衍射强度角谱 $I_p(\theta)$;(c)介质末端 $L=600\,\mu m$ 处的透射谱 $T(x)$。相关参数为 $\Omega_c/2\pi=3.0\,MHz$, $\Delta_p/2\pi=-2.27\,MHz$, $\Delta_{c0}/2\pi=-0.1\,MHz$, $\delta_{c0}/2\pi=1.0\,MHz$ 以及 $\Lambda_{icp}/2\pi=2.0\,MHz$

Fig. 2　Diffraction properties of PT antisymmetric grating. (a) Absorption (solid curve) and dispersion (dotted curve) spectra; (b) grating diffraction intensity angular spectrum $I_p(\theta)$; (c) transmission spectrum $T(x)$ at end of medium $L=600\,\mu m$, with relevant parameters $\Omega_c/2\pi=3.0\,MHz$, $\Delta_p/2\pi=-2.27\,MHz$, $\Delta_{c0}/2\pi=-0.1\,MHz$, $\delta_{c0}/2\pi=1.0\,MHz$, and $\Lambda_{icp}/2\pi=2.0\,MHz$

和 $\chi'(-x)=-\chi'(x)$。由于左半个周期 $-a/2<x<0$ 内存在光学增益[$\chi'(x)<0$],因此,图 2(c)显示了大于 1.0 的透射率。此时,极化率实部与虚部的空间调制正好处于反相调制,如图 2(b)所示,该电磁诱导光栅系统产生了非对称的衍射角谱。值得注意的是,该光学 PT 对称系统的实现仅仅采用了单重周期调制,对比双周期调制系统而言,降低了实现非厄密光学系统的复杂度。

3.2　宇称-时间反对称光栅

当参数为 $\Delta_p=\Delta_{c0}=0$、$\delta_{c0}=1.0\times2\pi\,MHz$ 以及 $\psi=0$ 时,如图 3(a_1)和 3(a_2)所示,原子体系极化率实部(点线)与虚部(实线)分别为空间位置 x 的奇函数与偶函数,即 $\chi'(-x)=-\chi'(x)$ 和 $\chi''(-x)=\chi''(x)$。与 PT 对称的情况相似,由于系统极化率实部与虚部相对于空间位置 x 反相调制,从而实现了非对称衍射,如图 3(b_1)和 3(b_2)所示。通常 PT 反对称光栅(APT-grating)的衍射能力弱于 PT 对称光栅。其原因在于 PT 反对称系统要求极化率实部为奇函数,即在共振位置附近的色散贡献较小,如果要获得非 0 级次较好的衍射效率,则需要较大的光学深度(O_D)。而对于非增益的 PT 反对称系统在共振位置附近是纯耗散的,大光学深度会导致过多的吸收从而导致非 0 级次衍射效率降低,因此,无法仅通过调控光学深度得到衍射能力较强的 PT 反对称光栅。但从图 3(b_1)可以看出,当前方案中的非增益 PT 反对称光栅($\Lambda_{icp}=0$)仅在 $\sin\theta=0.5$ 即 $\theta=30°$ 处产生了效率为 $I_p(30°)=0.24$ 的非对称衍射,这是一个尚可接受的结果。产生该结果的原因是,此系统在共振位置区域的吸收较小[如图 3(a_1)所示,$\chi'(x)\infty0$,当 $-a/4<x<a/4$ 时],即使在远离共振区域的位置介质也有 $T(x)>0.2$ 的整体透射率,如图 3(c_1)所示。图 3(a_2)、3(b_2)、3(c_2)则分别展示了开启非相干泵浦后($\Lambda_{icp}/2\pi=2.0\,MHz$),带有光学增益的 PT 反对称光栅的吸收色散曲线、带增益效果的非对称衍射角谱以及透射谱。在与纯耗散型光栅的比较中可以发现,系统此时的光学响应变化趋势是相似的,见图 3(a_1)~(c_1),且非对称光栅的单一级次衍射效率由于光学增益的原因,得到了有效的增强 $I_p(30°)=200$。

接下来进一步讨论影响该非厄密光学系统衍射性质的因素。首先,图 4(a)展示了 PT 反对称情况下,随光学深度逐渐增大($0<O_D<100$),耗散型 PT 反对称光栅(非相干泵浦速率为 $\Lambda_{icp}=0$)衍射角谱的变化,不难发现,光学深度增至 $O_D>30$,衍射强度几乎全部分布在 +1 级($\sin\theta=0.5$),随着光学深度进一步增加 $O_D>80$,耗散作用下 +1 级衍射强度逐步降低趋于 0。图 4(b)展示了增益型 PT 反对称光栅(非相干泵浦速率为 $\Lambda_{icp}/2\pi=2.0\,MHz$)衍射角谱的变化:与耗散型的前期变化趋势相似的是,随光学深度增加 $90<O_D<120$,衍射强度从 0 级向 +1 级转移。不同的是,光学增益保证了 +1 级衍射强度不会由于光学深度的增加而降低,衍射强度反而越来越大,由此可见,增益型 PT 反对称光栅即使在大光学深度下依然获得了可观的非对称衍射效果。进一步,图 4(c_1)与 4(c_2)展示了固定光学深度为 $O_D=130$ 时,随非相干泵浦速率 Λ_{icp} 增大时增益型 PT 反对称光栅的衍射角谱。非相干泵浦对光栅衍射分布的影响与光学深度的情况刚好相反:随非相干泵浦速率 Λ_{icp} 的增大 $\left(0<\frac{\Lambda_{icp}}{2\pi}<4.0\,MHz\right)$,衍射强度从 +1 级向 0 级转移;当 $\frac{\Lambda_{icp}}{2\pi}>4.3\,MHz$ 时,衍射光强几乎全部集中于 0 级次。其原因在于,非相干泵浦增加了|e⟩态的粒子数布居(原 EIT 条件下 $\rho_{ee}\approx0$),导致介质的色散曲线由陡峭变得平缓,即极化率实部对空间位置 x[以及频率 $\delta_p(x)$]的一阶偏导数降低,进而削弱了该光栅系统将光场向高级次衍射的能力。当 $\Lambda_{icp}\gg\delta_{c0}$ 时,失谐的空间调制对介质色散的影响则可以忽略不计,此时该光栅也失去了对探测光的衍射作用。需要指出的是,由于系统存在增益,衍射强度(效率)的绝对量是一直增加的,这里描述的转移是相对衍射强度 $I_p^N(\theta)=\frac{I^N{}_p(\theta)}{\int_{-\pi/2}^{+\pi/2}I_p(\theta)\mathrm{d}\theta}$ 的转移。因此,在一定区

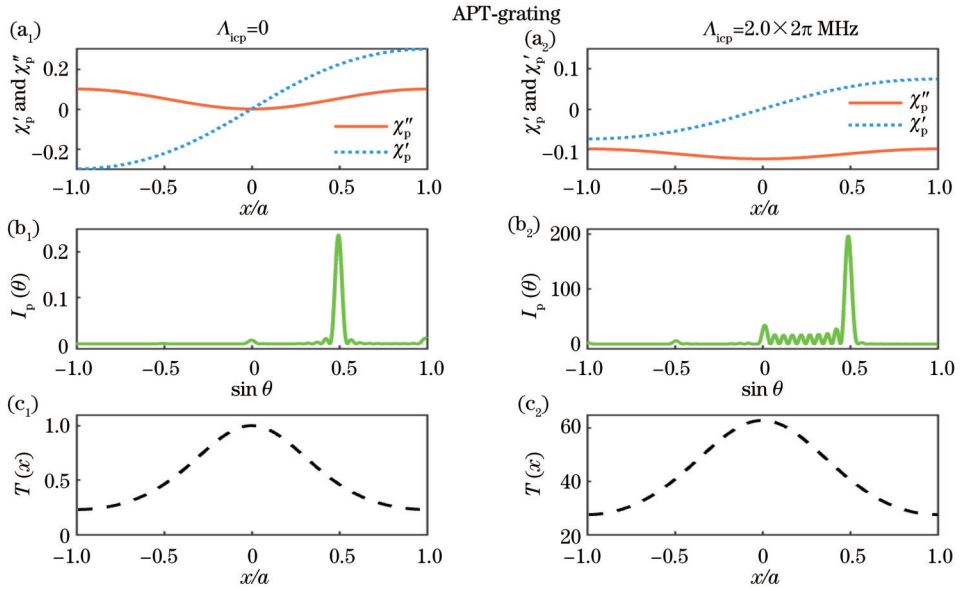

图 3　PT 反对称光栅衍射性质。(a_1)、(a_2)吸收(实线)与色散(点线)谱;(b_1)、(b_2) 光栅衍射强度角谱 $I_p(\theta)$;(c_1)、(c_2) 透射谱 $T(x)$。所有图中失谐取 $\Delta_p/2\pi=\Delta_{c0}/2\pi=0$,除($a_1$)~($c_1$)中取 $\Lambda_{icp}=0$ 和 $L=200\ \mu m$、(a_2)~(c_2)中取 $\Lambda_{icp}/2\pi=2.0$ MHz 和 $L=450\ \mu m$ 以外,其他参数与图 2 相同

Fig. 3　Diffraction properties of PT antisymmetric grating. (a_1), (a_2) Absorption (solid curve) and dispersion (dotted curve) spectra; (b_1), (b_2) grating diffraction intensity angular spectrum $I_p(\theta)$; (c_1), (c_2) transmission spectrum $T(x)$. Detuning here are chosen as $\Delta_p/2\pi=\Delta_{c0}/2\pi=0$, and other parameters are same as in Fig. 2 except (a_1)-(c_1) $\Lambda_{icp}=0$ with $L=200\ \mu m$ and (a_2)-(c_2) $\Lambda_{icp}/2\pi=2.0$ MHz with $L=450\ \mu m$

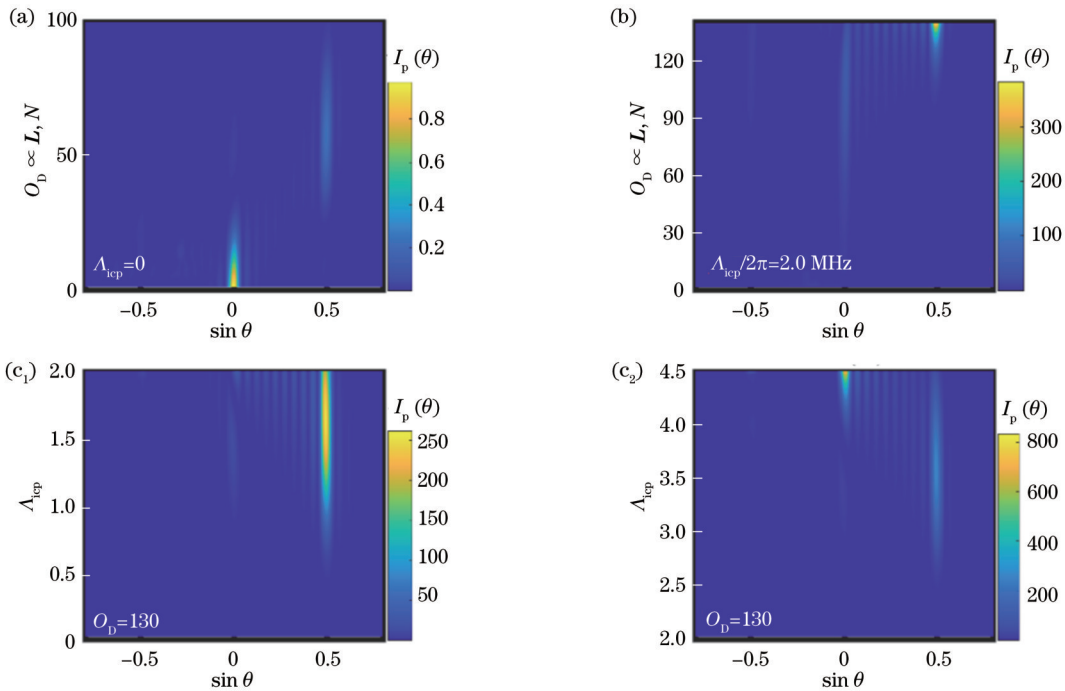

图 4　PT 反对称光栅的衍射谱。(a)、(b)随光学深度变化的衍射谱,此时的非相干泵浦速率分别取 $\Lambda_{icp}/2\pi=0$, 2.0 MHz;(c_1)、(c_2)随非相干泵浦变化的衍射谱,此时的光学深度为 $O_D=130$

Fig. 4　Diffraction spectra of PT antisymmetric grating. (a), (b) Diffraction spectra varying with optical depth (OD) with $\Lambda_{icp}/2\pi=0$, 2.0 MHz, respectively; (c_1), (c_2) diffraction spectra varying with incoherent pumping with $O_D=130$

间内,非相干泵浦可以作为一种新的有效手段,操控这种非对称光栅衍射强度分布的自由度。

固定光学深度,当介质长度取 $L=600\ \mu m$ 时,继续讨论非相干泵浦速率与耦合场失谐相位 φ 对光栅衍射性质的影响,如图 5 所示。比较图 5(a_1)~(c_1)、图 5(a_2)~(c_2),以及图 5(a_3)~(c_3)不难发现,随着非相干

泵浦的减弱，此时光栅有将探测光束衍射到更高衍射级次的趋势（从±1级→±2级）。比较图5(a_1)～(a_3)、图5(b_1)～(b_3)，以及图5(c_1)～(c_3)可以发现，控制场失谐相位ψ具有两种调控的功能：1）改变非对称衍射的方向，$\psi=0\rightarrow\psi=\pi$使得非对称衍射方向从负角度变至正角度；2）改变衍射的对称性，$\psi=m\pi\rightarrow\psi=(2m-1)\pi/2$使得光栅从非对称衍射变为对称衍射。

对于情况1），$\psi=0\rightarrow\psi=\pi$在$\Delta_{c0}=0$时，将$\psi=0\rightarrow\psi=\pi$相当于翻转$\Delta_c(x)=\delta_{c0}\sin[\pi(x-x_0)/(2a)]$的符号，进而改变极化率实部与虚部空间调制的相位差，因此可以实现非对称衍射方向的控制。对于情况2），$\psi=(2m-1)\pi/2$使得$\Delta_c(x)=\Delta_{c0}+\delta_{c0}\cos[\pi(x-x_0)/(2a)+m\pi]$，导致极化率实部与虚部在此空间调制下均为偶函数，不再满足光学PT对称或者PT反对称（不满足空间Kramers-Kronig关系）[40-43]，因此高阶衍射项不起作用，进而导致光栅衍射行为从非对称衍射向传统的对称衍射转变。

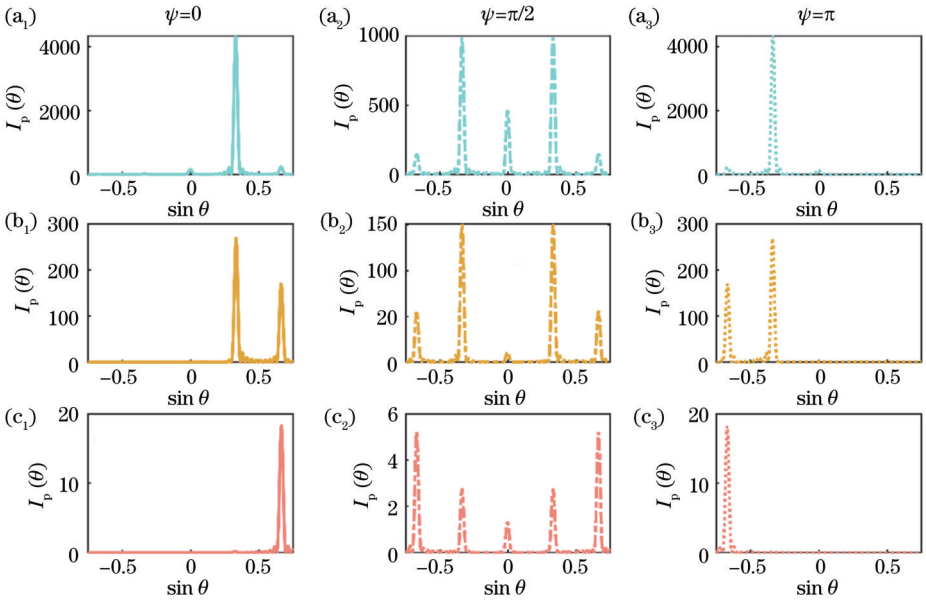

图5　非相干泵浦与控制场失谐相位对衍射谱的影响。非相干泵浦速率分别为(a_1)～(a_3)$\Lambda_{icp}/2\pi=1.5$ MHz；(b_1)～(b_3)$\Lambda_{icp}/2\pi=1.0$ MHz；(c_1)～(c_3)$\Lambda_{icp}/2\pi=0.5$ MHz；控制场失谐相位分别为(a_1)～(c_1)$\psi=0$；(a_2)～(c_2)$\psi=\pi/2$；(a_3)～(c_3)$\psi=\pi$。此时$L=600$ μm，$R=3$，其他参数均与图3相同

Fig. 5　Influence of incoherent pumping and phase of coupling field detuning on diffraction spectrum. Incoherent pumping rate is (a_1)-(a_3) $\Lambda_{icp}/2\pi=1.5$ MHz; (b_1)-(b_3) $\Lambda_{icp}/2\pi=1.0$ MHz; (c_1)-(c_3) $\Lambda_{icp}/2\pi=0.5$ MHz; coupling detuning phase is (a_1)-(c_1) $\psi=0$; (a_2)-(c_2) $\psi=\pi/2$; (a_3)-(c_3) $\psi=\pi$, with $L=600$ μm, $R=3$, and other parameters are same as in Fig. 3

表1汇总了本文基于非相干泵浦辅助的电磁诱导光栅方案的几种衍射类型与衍射模式，以及相关衍射类型的特性和调控对各个参数的要求。可以通过控制耦合场失谐中的相位ψ配合不同的非相干泵浦速率Λ_{icp}来实现包含3种非对称衍射（PT对称、耗散型PT反对称、增益型PT反对称）以及对称衍射共4种不同衍射模式之间的切换。除保留既往连续型非厄密光栅中光学深度这一调控自由度之外，该方案还引入了非相干泵浦速率以及控制场失谐相位作为对非厄密光栅衍射性调控的自由度。

表1　不同衍射类型与衍射模式及操控参数比较

Table 1　Comparison of different diffraction types and diffraction modes with several control parameters

Diffraction mode and non-Hermitian grating type	Asymmetric diffraction			Symmetric diffraction
	PT-grating	Loss-type APT grating	Gain-type APT grating	
Incoherent pumping ($\Lambda_{icp}/2\pi$ MHz)	2.0	0	>0	∀
O_D modulation	√	√	√	√
Phase (ψ/π)	$2m$	$2m$	$2m+1$	$(2m+1)/2$
Modulation by sign of detuning	×	√ Diffraction direction	√ Diffraction direction	—
Asymmetric degree	Unperfect	Perfect	Near perfect	—

4 结 论

本文提出了在非相干泵浦辅助的三能级Λ型冷原子系统中，利用驻波耦合的单重空间调制手段实现非厄密电磁诱导光栅的理论方案。在该方案中，通过调控探测场与控制场的频率失谐，可以实现该系统从光学PT对称性到PT反对称性的转变。通过操控非相干泵浦速率，可以获得两种不同类型的PT反对称性（耗散型与增益型），并且实现非对称的单一级次衍射效率的增益。在光学深度固定的情况下，改变非相干泵浦速率可以对光栅衍射性质进行操控（衍射级次之间的相对衍射效率比），为非厄密光栅的操控引入了新的自由度。通过控制场失谐相位调制，可以实现光栅系统对探测光非对称衍射方向的控制以及对光栅不同衍射模式（对称衍射或非对称衍射）的切换。本文提出的单重空间周期调制方案降低了制备非厄密光学介质的复杂度，配合控制场失谐相位与非相干泵浦速率的调制，可以实现对称衍射型、PT对称型、耗散PT反对称型以及增益PT反对称型等4种不同的衍射模式及其动态操控。因此，该研究结果将有效地促进非厄密光学以及散射型全光学器件的研究与发展，并在量子信息处理中具有广泛的应用前景。

参 考 文 献

[1] 唐原江, 梁超, 刘永椿. 宇称-时间对称与反对称研究进展[J]. 物理学报, 2022, 71(17): 171101.
Tang Y J, Liang C, Liu Y C. Research progress of parity-time symmetry and anti-symmetry[J]. Acta Physica Sinica, 2022, 71(17): 171101.

[2] Bender C M. Making sense of non-Hermitian Hamiltonians[J]. Reports on Progress in Physics, 2007, 70(6): 947-1018.

[3] Nguyen N B, Maier S A, Hong M H, et al. Recovering parity-time symmetry in highly dispersive coupled optical waveguides [J]. New Journal of Physics, 2016, 18(12): 125012.

[4] Eichelkraut T, Heilmann R, Weimann S, et al. Mobility transition from ballistic to diffusive transport in non-Hermitian lattices[J]. Nature Communications, 2013, 4: 2533.

[5] 党婷婷, 王娟芬. 高斯型PT对称波导中高斯光波的控制[J]. 光学学报, 2020, 40(3): 0319001.
Dang T T, Wang J F. Control of Gaussian optical waves in Gaussian parity-time symmetric waveguide[J]. Acta Optica Sinica, 2020, 40(3): 0319001.

[6] Peng B, Özdemir Ş K, Lei F C, et al. Parity-time-symmetric whispering-gallery microcavities[J]. Nature Physics, 2014, 10(5): 394-398.

[7] Chang L, Jiang X S, Hua S Y, et al. Parity-time symmetry and variable optical isolation in active-passive-coupled microresonators[J]. Nature Photonics, 2014, 8(7): 524-529.

[8] Choi Y, Hahn C, Yoon J W, et al. Observation of an anti-PT-symmetric exceptional point and energy-difference conserving dynamics in electrical circuit resonators[J]. Nature Communications, 2018, 9(1): 2182.

[9] Sheng J T, Miri M A, Christodoulides D N, et al. PT-symmetric optical potentials in a coherent atomic medium[J]. Physical Review A, 2013, 88(4): 041803.

[10] Ge L, Türeci H E. Antisymmetric PT-photonic structures with balanced positive- and negative-index materials[J]. Physical Review A, 2013, 88(5): 053810.

[11] Wu J H, Artoni M, La Rocca G C. Non-Hermitian degeneracies and unidirectional reflectionless atomic lattices[J]. Physical Review Letters, 2014, 113(12): 123004.

[12] Wu J H, Artoni M, La Rocca G C. Parity-time-antisymmetric atomic lattices without gain[J]. Physical Review A, 2015, 91(3): 033811.

[13] Peng P, Cao W X, Shen C, et al. Anti-parity-time symmetry with flying atoms[J]. Nature Physics, 2016, 12(12): 1139-1145.

[14] Longhi S. Bloch oscillations in complex crystals with PT symmetry[J]. Physical Review Letters, 2009, 103(12): 123601.

[15] Zhang Y Q, Zhang D, Zhang Z Y, et al. Optical Bloch oscillation and Zener tunneling in an atomic system[J]. Optica, 2017, 4(5): 571-575.

[16] Hodaei H, Miri M A, Heinrich M, et al. Parity-time-symmetric microring lasers[J]. Science, 2014, 346(6212): 975-978.

[17] Jing H, Özdemir S K, Lü X Y, et al. PT-symmetric phonon laser[J]. Physical Review Letters, 2014, 113(5): 053604.

[18] Feng L, Wong Z J, Ma R M, et al. Single-mode laser by parity-time symmetry breaking[J]. Science, 2014, 346(6212): 972-975.

[19] Lin Z, Ramezani H, Eichelkraut T, et al. Unidirectional invisibility induced by PT-symmetric periodic structures[J]. Physical Review Letters, 2011, 106(21): 213901.

[20] Feng L, Xu Y L, Fegadolli W S, et al. Experimental demonstration of a unidirectional reflectionless parity-time metamaterial at optical frequencies[J]. Nature Materials, 2013, 12(2): 108-113.

[21] Yin X B, Zhang X. Unidirectional light propagation at exceptional points[J]. Nature Materials, 2013, 12(3): 175-177.

[22] Sarısaman M, Tas M. Unidirectional invisibility and PT symmetry with graphene[J]. Physical Review B, 2018, 97(4): 045409.

[23] Krešić I, Makris K G, Leonhardt U, et al. Transforming space with non-Hermitian dielectrics[J]. Physical Review Letters, 2022, 128(18): 183901.

[24] Fleischhauer M, Imamoglu A, Marangos J P. Electromagnetically induced transparency: optics in coherent media[J]. Reviews of Modern Physics, 2005, 77(2): 633-673.

[25] Ling H Y, Li Y Q, Xiao M. Electromagnetically induced grating: homogeneously broadened medium[J]. Physical Review A, 1998, 57(2): 1338-1344.

[26] de Araujo L E E. Electromagnetically induced phase grating[J]. Optics Letters, 2010, 35(7): 977-979.

[27] Liu Y M, Tian X D, Wang X, et al. Cooperative nonlinear grating sensitive to light intensity and photon correlation[J]. Optics Letters, 2016, 41(2): 408-411.

[28] Asghar S, Ziauddin, Qamar S, et al. Electromagnetically induced grating with Rydberg atoms[J]. Physical Review A, 2016, 94(3): 033823.

[29] Zhang Y P, Wang Z G, Nie Z Q, et al. Four-wave mixing dipole soliton in laser-induced atomic gratings[J]. Physical Review Letters, 2011, 106(9): 093904.

[30] Liu Y M, Gao F, Fan C H, et al. Asymmetric light diffraction of an atomic grating with PT symmetry[J]. Optics Letters, 2017, 42(21): 4283-4286.

[31] Bushuev V A, Dergacheva L V, Mantsyzov B I. Asymmetric pendulum effect and transparency change of PT-symmetric photonic crystals under dynamical Bragg diffraction beyond the paraxial approximation[J]. Physical Review A, 2017, 95(3): 033843.

[32] Zhang Z Y, Yang L, Feng J L, et al. Parity-time-symmetric optical lattice with alternating gain and loss atomic configurations [J]. Laser & Photonics Reviews, 2018, 12(10): 1800155.

[33] Shui T, Yang W X, Liu S P, et al. Asymmetric diffraction by atomic gratings with optical PT symmetry in the Raman-Nath regime[J]. Physical Review A, 2018, 97(3): 033819.

[34] Ma D D, Yu D M, Zhao X D, et al. Unidirectional and controllable higher-order diffraction by a Rydberg

electromagnetically induced grating[J]. Physical Review A, 2019, 99(3): 033826.
[35] Liu Y M, Gao F, Wu J H, et al. Lopsided diffractions of distinct symmetries in two-dimensional non-Hermitian optical gratings[J]. Physical Review A, 2019, 100(4): 043801.
[36] Hang C, Li W B, Huang G X. Nonlinear light diffraction by electromagnetically induced gratings with PT symmetry in a Rydberg atomic gas[J]. Physical Review A, 2019, 100(4): 043807.
[37] Gao J, Hang C, Huang G X. Linear and nonlinear Bragg diffraction by electromagnetically induced gratings with PT symmetry and their active control in a Rydberg atomic gas[J]. Physical Review A, 2022, 105(6): 063511.
[38] Yang Y Z, Jia H, Bi Y F, et al. Experimental demonstration of an acoustic asymmetric diffraction grating based on passive parity-time-symmetric medium[J]. Physical Review Applied, 2019, 12(3): 034040.
[39] Hua S, Liu Y M, Lio G E, et al. Tailored diffraction asymmetries from spatially odd-symmetric phase gratings[J]. Physical Review Research, 2022, 4(2): 023113.
[40] Horsley S A R, Artoni M, La Rocca G C. Spatial Kramers-Kronig relations and the reflection of waves[J]. Nature Photonics, 2015, 9(7): 436-439.
[41] Ye D X, Cao C, Zhou T Y, et al. Observation of reflectionless absorption due to spatial Kramers-Kronig profile[J]. Nature Communications, 2017, 8(1): 1-10.
[42] Baek Y, Park Y. Intensity-based holographic imaging via space-domain Kramers-Kronig relations[J]. Nature Photonics, 2021, 15(5): 354-360.
[43] Zhang Y, Wu J H, Artoni M, et al. Controlled unidirectional reflection in cold atoms via the spatial Kramers-Kronig relation [J]. Optics Express, 2021, 29(4): 5890-5900.

Electromagnetically Induced Non-Hermitian Diffraction Grating Assisted by Incoherent Pumping

Tian Xuedong[1], Liu Xingyu[2], Liu Yimou[2*]

[1]*College of Physics Science and Technology, Guangxi Normal University, Guilin* 541004, *Guangxi, China*;
[2]*Center for Quantum Sciences, Northeast Normal University, Changchun* 130024, *Jilin, China*

Abstract

Objective A system with non-Hermitian Hamiltonian commutative with the parity-time operator, proposed by Bander et al., has a real eigenenergy spectrum and some novel properties under certain conditions. Due to the similarity between Schrodinger′s equation and the optical Helmholtz equation, the optical system with out-of-phase spatial modulation is a good platform to simulate a system with parity-time (PT) symmetry, which is named the non-Hermitian optical system. In recent years, non-Hermitian optical structures based on discrete systems such as optical waveguide, hybrid optical microcavity, electrical circuit resonators, and continuous optical media such as cold atomic ensemble with spatially periodic modulation, have been implemented successively in experimental and theoretical studies. Spectroscopic devices such as diffraction grating have been a significant branch of optical devices since Newton′s era. Electromagnetically induced grating (EIG) based on electromagnetically induced transparency (EIT) makes it possible to tune the diffraction patterns dynamically. In recent years, combined with the non-Hermitian optical modulation, many schemes of one- or two-dimensional asymmetric optical diffraction gratings have been proposed successively. However, due to rigid realization conditions of PT symmetry or PT antisymmetry, there is still a great hindrance to realizing precise and flexible dynamic operation, especially for some special optical diffractions. In most previous schemes, dual spatial periodic modulation (via amplitude, detuning of coupling field, or atomic density) has been adopted to achieve two goals, including the realization of PT symmetry or PT antisymmetry and the construction of a grating structure. This results in the lack of accurate modulation capabilities with the protection of PT symmetry or PT antisymmetry. Therefore, a method for preparing non-Hermitian EIG with simple structures easy to analyze, dynamic control ability, and protection of optical non-Hermitian symmetry is necessary and desired.

Method We consider an ensemble of cold ^{87}Rb atoms driven into a three-level Lambda configuration by two coherent fields with frequencies ω_p and ω_c. The weak probe field ω_p interacts with transition $|g\rangle \leftrightarrow |e\rangle$, while the strong control field ω_c acts upon transition $|m\rangle \leftrightarrow |e\rangle$. The states $|g\rangle$ and $|e\rangle$ are coupled by the incoherent pumping Λ_{icp} additionally. By periodically modulating the coupling field detuning $\Delta_c(x)$, it is possible to get an asymmetric diffraction pattern in this system.

Results and Discussions According to the study on far-field diffraction characteristics of probe field through the system, some results are as follows. 1) When the parameters are chosen as $\Delta_p = -2.27\times 2\pi$ MHz, $\Delta_{c0} = -0.1\times 2\pi$ MHz, $\delta_{c0} = 1.0\times 2\pi$ MHz and $\psi = 0$, we can get the PT symmetric susceptibility. Then the modulations for the real part and

imaginary part of the susceptibility are out-of-phase, and the lopsided diffraction patterns are shown in Fig. 2(b). 2) When the parameters are chosen as $\Delta_p=\Delta_{c0}=0$, $\delta_{c0}=1.0\times2\pi$ MHz, and $\psi=0$, we can get the PT antisymmetric susceptibility. The modulations for the real part and imaginary part of the susceptibility are still out-of-phase, resulting in the lopsided diffraction patterns shown in Figs. 3(b_1) and 3(b_2). 3) With increasing optical depth, the diffracted intensity is transferred from zero order to one order, while with increasing incoherent pumping, the diffracted intensity is transferred from one order to zero order in the PT antisymmetric grating as shown in Fig. 4. 4) The initial phase of coupling field detuning can modulate the diffraction in two ways. The first one is changing the diffraction direction from a negative angle to a positive angle by varying the initial phase of the coupling field detuning from 0 to π. The other one is tuning the diffraction symmetries of the grating. When $\psi=m\pi$, we can get asymmetric diffraction patterns, and when $\psi=(2m-1)\pi/2$, we can get symmetric diffraction patterns shown in Fig. 5.

Conclusions We propose a theoretical scheme of non-Hermitian electromagnetically induced grating based on incoherent pumping. The system consists of an ultra-cold atomic ensemble with the Lambda-type three-level structure and an incoherent pumping field. Combined with incoherent pumping, non-Hermitian symmetries of the system including optical PT symmetry and PT antisymmetry under the single spatial period modulation can be implemented. During the research on far-field diffraction characteristics of probe field through the system, we can draw the following conclusions. First, a switch between different non-Hermitian optical symmetries can be attained by controlling the detuning of the coupling field. Secondly, the diffraction efficiency is effectively modulated by incoherent pumping at a constant optical depth, which introduces a new degree of freedom of grating manipulation. In addition, tuning the initial phase of coupling field detuning can effectively modulate the diffraction symmetry and diffraction pattern of the system. The theoretical results not only can facilitate the research and development of non-Hermitian optics and scattering-type all-optical devices but also can be applied in quantum optics and quantum information processing.

Key words diffraction and grating; electromagnetically induced transparency; non-Hermitian optics; incoherent pumping; diffraction grating; asymmetric diffraction